UCRL-102036
PREPRINT

FORMATION OF NIOBIUM CARBIDES IN HIGH-DOSE CARBON-ION-IMPLANTED AND ANNEALED NIOBIUM

J. S. Huang

This paper was prepared for submittal to
Materials Research Society 1989 Fall Meeting
Symposium A, Beam-Solid Interactions: Physical Phenomena
Boston, MA, Nov. 27–Dec. 1, 1989

October 30, 1989

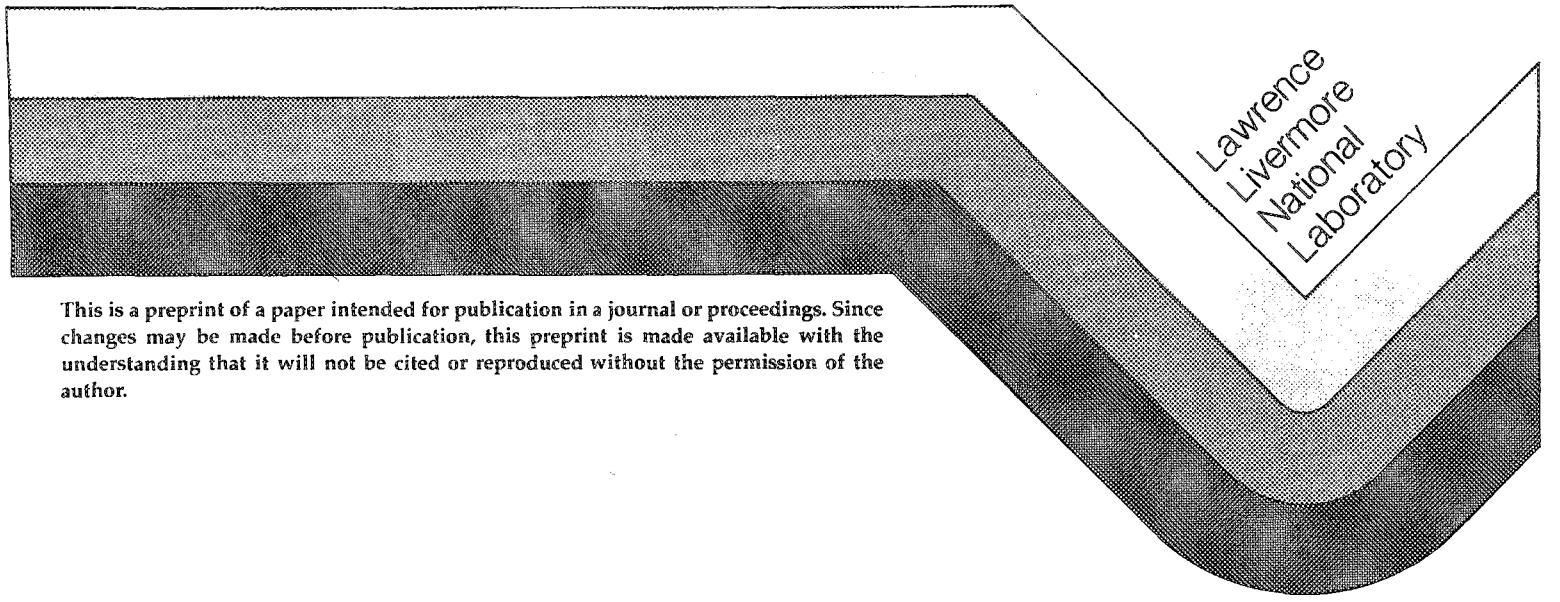

FORMATION OF NIOBIUM CARBIDES IN HIGH-DOSE CARBON-ION-IMPLANTED AND ANNEALED NIOBIUM

J. S. HUANG
Lawrence Livermore National Laboratory, P.O. Box 808, Livermore, CA 94551

UCRL--102036

DE90 003601

ABSTRACT

Polycrystalline niobium was implanted with 200-keV C^+ ions to a total fluence of 7×10^{17} carbon ions per cm^2 (C/cm^2). Auger electron spectroscopy (AES) analysis showed that the carbon concentration varied from 5 to 50 at.% within a depth of about 4000 Å. Glancing-angle x-ray diffraction analysis (XRDA) and transmission electron microscopy (TEM) analysis indicated that no Nb_2C phase was formed and that a buried fcc NbC layer was formed in the region where carbon content exceeds about 40 at.%. The absence of Nb_2C was attributed to the low diffusivity of carbon atoms and the fact that it could form only as an intermetallic compound. As a result of the TEM analysis and the fact that the diffusivity of carbon is very small, the formation of NbC is described as a type of diffusionless martensitic transformation. When the implanted samples were annealed at 1273 K for 1 h, the implanted carbon redistributed, the NbC phase disappeared, and an orthorhombic Nb_2C phase formed as spherical precipitates.

INTRODUCTION

Surface modification of metals by ion implantation is a technology with great commercial potential. The process usually results in the formation of a metastable phase on the modified surface with novel chemical or mechanical properties. Formation of the metastable phase can usually not be predicted based on the laws of classical thermodynamics (e.g., the Gibbs phase rule) and, therefore, requires experimental study for each individual system. Implantation of metalloid atoms into metal is of significant interest because it usually improves the fatigue and wear resistance of the metal.

Although a significant amount of work has been conducted on the implantation of metalloid ions such as carbon and nitrogen into iron alloys, little has been done on niobium and its alloys. In a previous work [1], we studied the implantation of carbon atoms into niobium up to a concentration of about 16 at.% carbon. We found that the formed metastable phase was a bcc niobium lattice with extended solubility for carbon and that no equilibrium Nb_2C and NbC phases were formed.

In this work, we extend the study to a higher dose, 7×10^{17} C/cm^2, which corresponds to a carbon concentration of about 44 at.% (calculated by TRIM [2]). The objectives are to understand at what composition any of the carbide phases will be formed and to understand the stability of the formed metastable phase when it is exposed to high temperature.

EXPERIMENTAL DETAILS

The niobium was a commercial grade material of 99.9 wt% purity with a carbon content less than 0.003 wt%. The material was annealed at 1273 K for 1 h and mechanically polished to a finish of 0.1 μm before carbon implantation. The as-annealed material had an average grain size of 40 μm. The carbon-ion implantation was conducted with 200-keV C^+ ions near room temperature (<423 K). The maximum total fluence was 7.0×10^{17} C/cm^2, and the typical current density of the rastered beam was about 4 $\mu A/cm^2$. The vacuum in the sample chamber was about 10^{-4} Pa during implantation.

We characterized the implanted sample by Auger electron spectroscopy (AES) with 3-keV electrons at a current of 0.033 μA to determine the depth profile of carbon and niobium. We sputtered the sample with a 4-keV Ar^+ ion beam at a beam current of 0.174 μA. To determine the content of carbon and niobium from the AES analysis, we fabricated an NbC standard by

carburizing a niobium substrate in a mixture of 5% methane and 95% argon. By x-ray diffraction, we determined the lattice constant of the NbC standard to be 4.473 Å, which is very close to the reported value [3–5] of 4.470 Å for the NbC phase with 50 at.% carbon. Assuming the AES analysis sensitivity factor for the niobium MNN peak to be 0.27 [6], we determined the sensitivity factor for the carbon KLL peak to be 0.245 with a standard deviation of 0.0235.

To characterize the crystalline phases formed, we used TEM and glancing-angle-incidence copper XRDA at an incidence angle of 6°. We calculated that about 33% of the total x-ray signal was from the implanted region. In preparing cross-sectional TEM samples for the TEM analysis, we used an ion-milling technique in the final stage of thinning to obtain perforated holes and thin areas from mechanically polished slices. In the ion-milling process, the sample holder was chilled by liquid nitrogen. We used a JEOL-200CX scanning transmission electron microscope, which has an ultra-thin-window, energy-dispersive, x-ray detector. After implantation, the sample was annealed at 1273 K for 1 h in a vacuum of about 1.3×10^{-5} Pa.

EXPERIMENTAL RESULTS

Figure 1 shows the carbon concentration vs sputtering time for an as-implanted sample. Except for the region near the surface, the carbon concentration increases from about 10 at.% to a maximum of about 50 at.%, which is larger than the 44 at.% we calculated using TRIM [2]. The enrichment of carbon near the surface can be attributed to hydrocarbon contamination. Figure 1 also shows carbon content vs depth for the annealed sample. In this sample, the carbon atoms have migrated and have become more uniformly distributed, and the maximum carbon concentration is about 35 at.%, very close to the composition of Nb_2C.

The d-spacings of diffracting planes identified from XRDA are tabulated in Table I and compared with those of niobium (bcc), NbC (fcc), β-Nb_2C (high-temperature hcp phase) and α-Nb_2C (low-temperature orthorhombic phase). The presence of peaks at 2.58, 2.22, and 1.28 Å for the as-implanted sample strongly indicates the formation of the NbC phase. Since the peaks near 2.68, 2.48, 1.83, and 1.41 Å for both of the Nb_2C phases were not detected, it is certain that none of the Nb_2C phases was formed after the implantation, despite the fact that the amount of carbon exceeded the stoichiometric composition of 33.3 at.% carbon. In the post-implantation annealed sample, the NbC phase disappeared and was replaced with an Nb_2C phase, evidenced by the presence of peaks at 2.68, 1.82, 1.56, and 1.41 Å.

Figure 2 shows a TEM bright-field micrograph of the microstructure of the as-implanted sample and its associated selected-area diffraction pattern. The maximum range of ion implantation appears to be between 3500 and 4000 Å, close to that calculated by TRIM. A buried layer of NbC phase has been formed. The layer is about 1300 Å thick and is centered at a depth of about 2600 Å. The diffraction analysis indicates the NbC phase has an fcc structure with the ⟨100⟩ orientation being parallel to the electron-beam axis. We have not detected the presence of an Nb_2C phase. This agrees with the XRDA results. The calculated d-spacing for the NbC{020} planes is

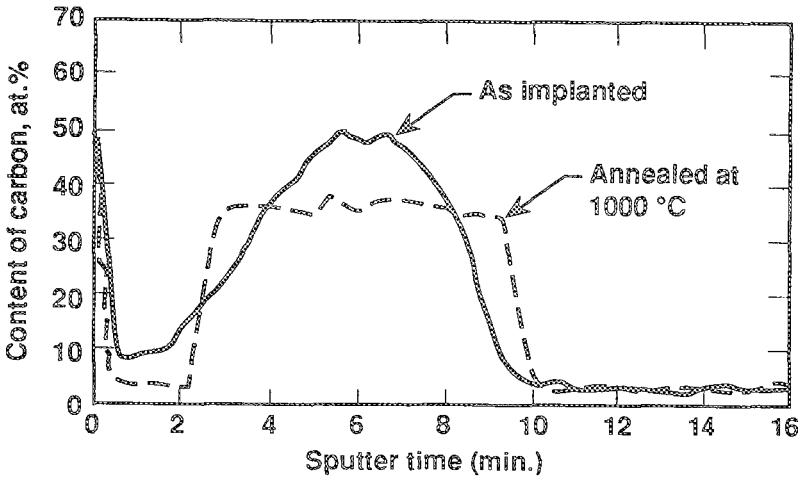

Fig. 1. AES depth profile of carbon for the as-implanted and post-implantation-annealed sample.

2.23 Å and is consistent with the value tabulated in Table I. The diffraction pattern can be indexed as a diffraction because of the combination of the fcc NbC phase with [100] orientation and the bcc niobium phase with [1$\bar{1}$0] orientation. By comparing the depth profile of carbon in Fig. 1 with the phase distribution in the TEM micrograph in Fig. 2, and assuming that the center of the NbC layer corresponds to the position of maximum carbon content, we estimate that the NbC phase is formed in the region where the concentration of carbon is greater than 40 at.%.

Table I. Sample d-spacings (Å) compared with those of niobium [7], NbC [8], α-Nb_2C (orthorhombic) [9], and β-Nb_2C (hcp) [10] phases.

Niobium	NbC	α-Nb_2C	β-Nb_2C	Implanted	Annealed
			4.250		
			3.680		
			2.720		
		2.682	2.683		2.68
	2.581			2.58	
		2.468	2.480		
			2.386		
2.338		2.349	2.363	2.35	2.35
	2.235			2.22	
			1.834		1.82
		1.811	1.828		
					1.67
1.653					1.65
	1.580				
			1.567		1.56
		1.551			
			1.547		
			1.415		1.41
		1.405	1.410		
			1.363		
1.350	1.348	1.344	1.346	1.35	1.35
			1.326		
		1.316	1.315		1.32
	1.290	1.299	1.299	1.28	
			1.244		
		1.237			
			1.195	1.19	
1.169		1.183	1.183	1.16	1.17
			1.131		
		1.124	1.128		1.13
	1.118				
					1.07
1.046			1.054	1.05	1.05
	1.043	1.044			1.04
	1.025			1.03	1.02
			1.021		
		1.018	1.014		1.01
			1.007		
			1.002		
	0.999	0.995	0.993		
			0.974		0.98
0.955					

Figure 3 shows a TEM bright-field micrograph of the microstructure of the annealed sample and its associated selected-area diffraction pattern. Note that the NbC layer has disappeared and many precipitates have formed. The diffraction pattern obtained from an area in the precipitates indicates that they are the α-Nb_2C phase. The calculated d-spacings for the $(0\bar{4}0)$ and $(00\bar{2})$ planes are 2.74 and 2.49 Å, respectively, which are close to the values reported in Table I. Note also that the α-Nb_2C phase has a long-range-ordered crystal structure, as evidenced by the superlattice spots for {001} planes in the pattern.

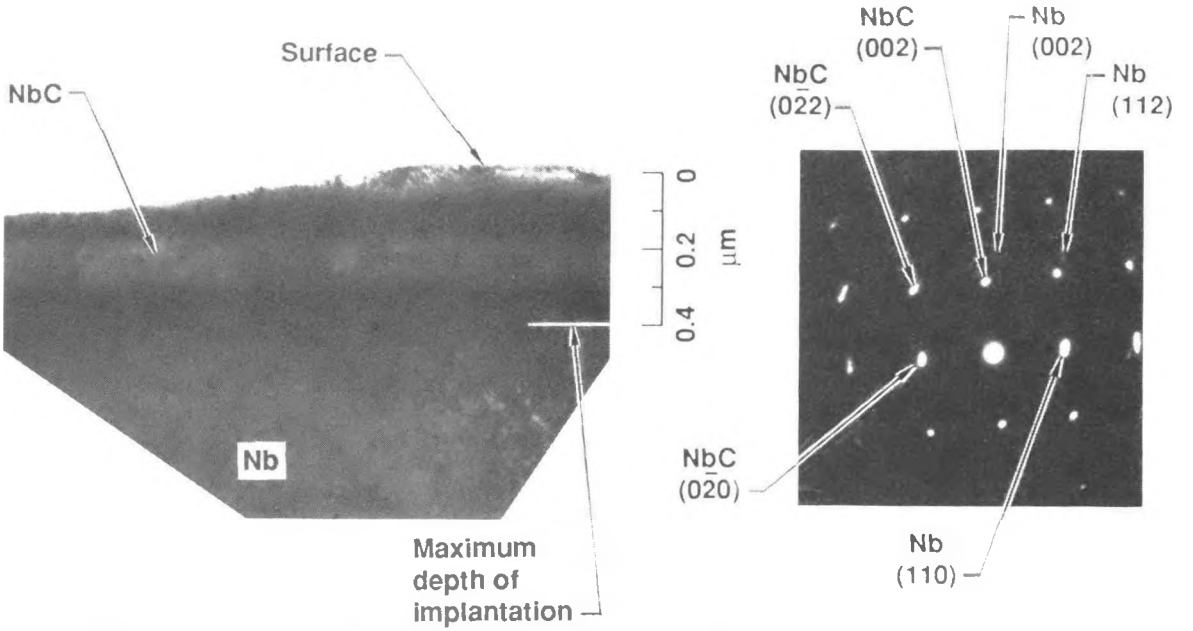

Fig. 2. Bright-field cross-sectional TEM micrograph and diffraction pattern for the as-implanted sample, showing the formation of the NbC phase and its orientation in relation to niobium.

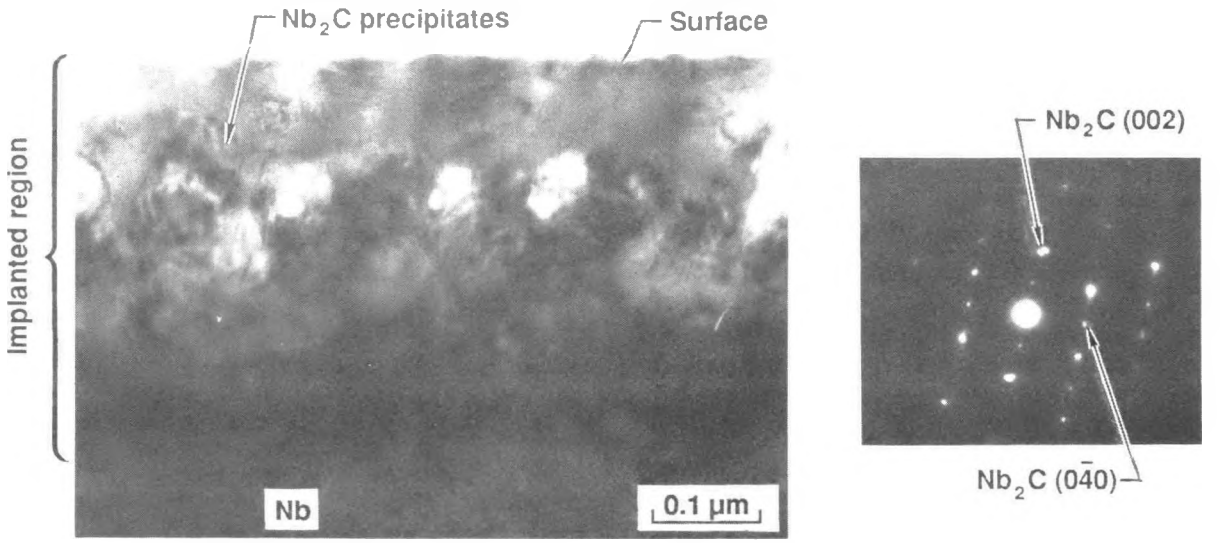

Fig. 3. Bright-field cross-sectional TEM micrograph and diffraction pattern for the post-implantation annealed sample, showing the formation of the Nb_2C phase, which has an ordered orthorhombic structure.

DISCUSSION

While our previous work [1] showed that Nb_2C does not form when the carbon concentration is as high as 16 at.%, our current work further shows that Nb_2C does not form even when the concentration is as high as 50 at.%. On the other hand, the NbC phase does form at compositions exceeding about 40 at.%. The equilibrium phase diagram also seems to imply a difference in the basis for forming NbC and Nb_2C. Based on the phase diagram, we find that Nb_2C exists only at compositions near 35 at.% carbon, while the NbC phase can exist with a wider range of compositions between 40 and 50 at.% carbon. The depth profile of carbon in the as-implanted sample indicates that the composition corresponding to 35 at.% carbon exists only at a certain depth. If the Nb_2C phase does form, it will do so as a plane with zero volume. The total free-energy change for the transformation will then be positive because of the interface formed between Nb_2C and niobium. Furthermore, Pedraza and Pedraza [11] showed that the formation of the Nb_2C phase requires a large amount of plastic energy caused by volume expansion. From a thermodynamic viewpoint, a transformation with free-energy increase will not occur.

Powers and Doyle [12] measured the diffusivity of carbon in niobium. The diffusion coefficient of carbon in niobium at 423 K (the maximum temperature during implantation) is 3.5×10^{-24} m^2/s. Within the duration of our ion implantation (about 8 h), the maximum distance of carbon travel is about 4 Å, which is less than the size of a unit cell of the low-temperature orthorhombic Nb_2C phase. Because of this low diffusivity of carbon, very little migration of carbon occurs after implantation to form the Nb_2C phase. On the other hand, when the sample was annealed for 1 h at 1273 K, the much higher mobility of carbon resulted in a buried region with composition near 35 at.% carbon, and precipitation of Nb_2C occurred. It should be noted that thermodynamics predicts the dissolution of the NbC phase, as the free energy of formation for Nb_2C is likely to be larger than that for NbC [13]. At 1273 K, there is no more kinetics constraint; therefore, the thermodynamic prediction agrees with our experimental observation.

The situation for the formation of NbC appears to be quite different. NbC has an fcc structure, with the carbon atoms existing as octahedral interstitials. For bcc niobium, the implanted carbon is probably located at its octahedral interstitial sites. However, the bcc lattice can be considered to be a face-centered tetragonal (fct) lattice, and the octahedral interstitial sites in the fct are the same as those in the bcc niobium lattice; therefore, the transformation from the carbon-implanted bcc niobium into an fcc NbC structure does not require long-range diffusion of carbon and niobium atoms, except for some lattice distortion. This transformation, also described as Bain transformation [14], is analogous to the opposite of the martensitic transformation in steels, where the fcc iron lattice transforms to a body-centered tetragonal (bct) iron lattice. It can be noted that for a Bain transformation (bcc→fct) without the aforementioned lattice distortion, the following crystallographic-direction relations should exist: $[1\bar{1}0]_{bcc} \rightarrow [100]_{fcc}$; $[110]_{bcc} \rightarrow [020]_{fcc}$; $[002]_{bcc} \rightarrow [002]_{fcc}$. However, the diffraction pattern in Fig. 2 indicates that the $[110]_{Nb}$ and $[002]_{Nb}$ directions are off from $[020]_{NbC}$ and $[002]_{NbC}$ by a few (~5) degrees. This is similar to the martensitic transformation in many steels where, in order to preserve an undeformed plane (habit plane), an additional deformation, involving a rotation of the crystal lattice, has to occur. This rotation is usually accomplished by dislocation slip or twinning. The evidence for dislocation slip or twinning can be seen in many substructures of the dark-field TEM image of the NbC phase in Fig. 4. There, the many traces of lines are likely caused by dislocation slip or twinning occurring on $\langle \bar{1}1\bar{1} \rangle \{112\}$ systems of the niobium bcc lattice or, equivalently, on the NbC fcc lattice $\langle 0\bar{2}2 \rangle \{022\}$ systems. Based on the above analysis, we conclude that the observed niobium→NbC formation is a type of martensitic transformation.

ACKNOWLEDGMENTS

We appreciate the assistance of R. Patterson in conducting the ion implantation, B. Olsen and M. A. Wall in the TEM analysis, and A. Connor in the AES analysis. The stimulating discussion provided by R. Musket is also appreciated. Work performed under the auspices of the U.S. Department of Energy by the Lawrence Livermore National Laboratory under contract W-7405-Eng-48.

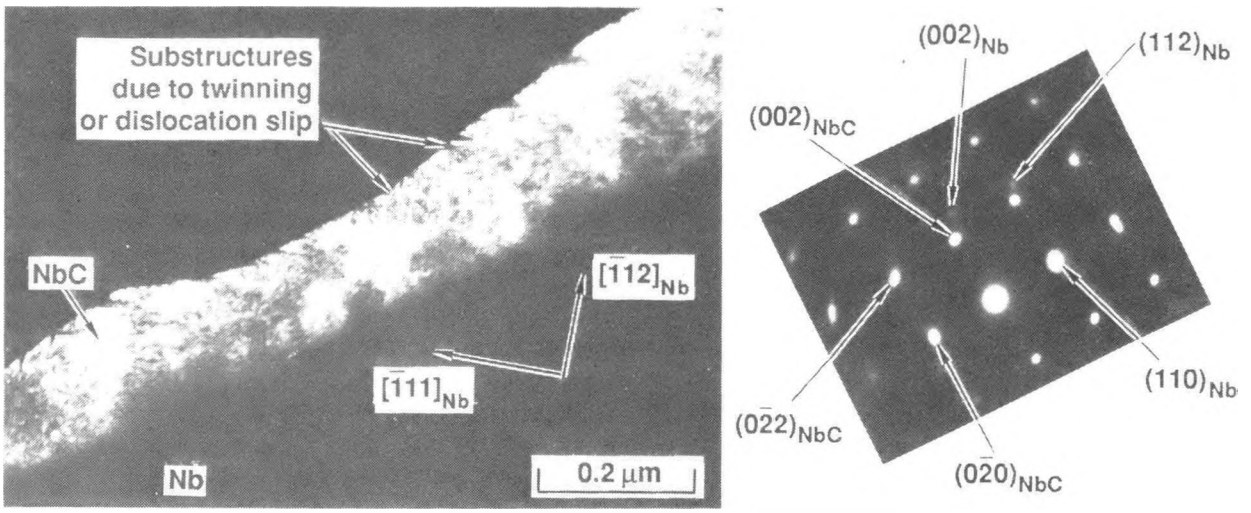

Fig. 4. Dark-field TEM image of the buried NbC layer formed from the implantation. Note the presence of twinning or shear-like substructures.

REFERENCES

1. J. S. Huang, R. G. Musket, and M. A. Wall, in*Processing Characterization of Materials Using Ion Beams*, *Mater. Res. Soc. Proc.*, Vol. 128, edited by L. E. Rhen, J. E. Greene, and F. A. Smidt (Materials Research Society, Pittsburgh, Pa., 1986), pp. 327–332.
2. Z. F. Ziegler, J. P. Biersack, and U. Littmark, *The Stopping and Range of Ions in Solids*, Vol. 1 (Pergamon Press, New York, 1985).
3. R. P. Elliott, *Trans. Am. Soc. Met.* **53**, 13 (1961).
4. E. K. Storms, *The Refractory Carbides* (Academic Press, New York, 1967).
5. K. Ono and J. Moriyama, *J. Less-Common Met.* **79**, 255 (1981).
6. L. E. Davis, N. C. MacDonald, P. W. Palmberg, G. E. Riach, and R. E. Weber, *Handbook of Auger Electron Spectroscopy*, 2nd ed. (Physical Electronics Industries, Eden Prairie, Minn., 1976).
7. *Nat. Bur. Stand. (U.S.) Monogr.* **25**, 21 (1984).
8. W. Wong-Ng, H. McMurdie, B. Paretzkin,C. Hubbard, and A. Dragoo, *JCPDG Grant-in-Aid Report* (U.S. Bureau of Standards, Washington, D. C., 1986).
9. E. Rudy and C. E. Brukl., *J. Am. Ceram. Soc.* **50**, 265 (1967).
10. *JCPDS Powder Diffraction Files*, PDF 15-127 (U.S. Bureau of Standards, Washington, D. C., 1988).
11. A. J. Pedraza and D. Pedraza, *Nucl. Instrum. Meth./Phys. Res.* **B16**(2,3), 270 (1986).
12. R. W. Powers and M. V. Dolyle, *J. Appl. Phys.* **30**, 514 (1959).
13. E. J. Huber et al., *J. Phys. Chem.* **65**, 1846 (1961).
14. E. C. Bain, *Trans. AIME* **70**, 25 (1924).